Journal of ELECTRONIC MATERIALS, Vol. 43, No. 8, 2014
DOI: 10.1007/s11664-014-3080-y

Antimonide-Based Type II Superlattices: A Superior Candidate for the Third Generation of Infrared Imaging Systems

M. RAZEGHI,[1,2] A. HADDADI,[1] A.M. HOANG,[1] G. CHEN,[1] S. BOGDANOV,[1] S.R. DARVISH,[1] F. CALLEWAERT,[1] P.R. BIJJAM,[1] and R. MCCLINTOCK[1]

1.—Electrical Engineering and Computer Science Department, Center for Quantum Devices, Northwestern University, Evanston, IL 60208, USA. 2.—e-mail: razeghi@eecs.northwestern.edu

Type II superlattices (T2SLs), a system of interacting multiquantum wells, were introduced by Nobel Laureate L. Esaki in the 1970s. Since then, this material system has drawn a lot of attention, especially for infrared detection and imaging. In recent years, the T2SL material system has experienced incredible improvements in material growth quality, device structure design, and device fabrication techniques that have elevated the performance of T2SL-based photodetectors and focal-plane arrays (FPAs) to a level comparable to state-of-the-art material systems for infrared detection and imaging, such as mercury cadmium telluride compounds. We present the current status of T2SL-based photodetectors and FPAs for imaging in different infrared regimes, from short wavelength to very long wavelength, and dual-band infrared detection and imaging, as well as the future outlook for this material system.

Key words: Infrared imaging, InAs/GaSb/AlSb type II superlattices, infrared photodetectors, high operating temperature, dual-band, focal-plane arrays

INTRODUCTION

The idea of antimonide-based type II superlattices (T2SLs) was first proposed by Sai-Halasz and Esaki in the 1970s.[1] The superlattice is formed by alternating InAs and GaSb layers over several periods. The type II broken-gap energy band alignment leads to separation of electrons and holes into the InAs and GaSb layers, respectively. This charge transfer gives rise to a high local electric field and strong interlayer tunneling of carriers without the requirement for an external electric field or additional doping. Large-period type II superlattices behave like semimetals, but if the superlattice period is shortened, the quantization effects are enhanced, causing a transition from a semimetal to a narrow-bandgap semiconductor. This narrow-bandgap semiconductor is suitable for both detection and emission in the infrared region. The resulting energy gaps depend upon the layer thicknesses and interface compositions, providing an enormous degree of freedom and robustness to device designers.

The T2SL material system has several advantages over other materials used for infrared detection and imaging technologies.[2] However, compared with state-of-the-art mercury cadmium telluride (MCT) compounds and most of the narrow-bandgap semiconductors that have very small electron and hole effective masses, the effective mass in T2SLs is relatively large, due to its special design which involves the interaction of electrons and holes via tunneling through adjacent barriers. Larger effective mass reduces the tunneling current in different devices such as photodiodes, which can be a major contributor to the dark current of MCT photodetectors. Moreover, Auger recombination, which is a limiting factor for high-temperature operation of infrared photodetectors, can be suppressed by manipulation of the energy band structures.[3] The capability of band-structure engineering opens the

(Received October 21, 2013; accepted February 13, 2014; published online March 18, 2014)

horizon for exploring novel device structures that are unthinkable using binary or ternary compound semiconductor band alignments such as in conventional MCT. A good example of this aspect is the M-structure superlattice (SL), with large effective mass and large tunability of band-edge energies,[4] which has been proposed as a novel variant of T2SLs. This structure has been shown to efficiently reduce the dark current in infrared photodiodes based on T2SLs. Thanks to all these fundamental properties, T2SLs have experienced rapid development over the past decade, with performance reaching a level comparable to state-of-the-art MCT-based infrared photodetectors.

In this paper, we review the current status of state-of-the-art type II superlattice-based photodetectors and focal-plane arrays (FPAs) for single- and dual-band detection and imaging in different infrared regimes and the outlook for this material system.

PHOTODIODES AND FOCAL-PLANE ARRAYS FROM SHORT- TO VERY LONG-WAVELENGTH INFRARED IMAGING

Short-Wavelength Infrared Photodetectors

The main challenge for short-wavelength infrared (SWIR) detection is the proper type II superlattice design with a cutoff wavelength between 1 μm and 3 μm. In a conventional InAs/GaSb T2SL, forming a large bandgap requires a thin InAs layer to push up the conduction band. The strained InSb interface will therefore result in lattice mismatch and prevent growth of thick structures to reach high quantum efficiency. Thus, the M-SL design was chosen instead of conventional InAs/GaSb T2SLs. In the M-structure, an AlSb layer is inserted into the GaSb layer, which pushes down the valence band and increases the bandgap of the superlattice. This superlattice design is still considered as a type II superlattice, because the electron excitation from valence band to conduction band still happens at the InAs/GaSb interface. The new superlattice design is lattice-matched to GaSb substrate, resulting in successful demonstration of T2SL-based SWIR photodetectors.[5] By reducing the InAs and GaSb layer thicknesses and increasing the AlSb layer thickness, we have been able to create high-quality T2SLs capable of SWIR detection with cutoff wavelengths down to 1.5 μm.

At 150 K, the photodiodes exhibited a dark current density of 5.6×10^{-8} A/cm^2 and a quantum efficiency of 40.3% in the front-side illumination configuration, resulting in an associated shot noise detectivity of 1.0×10^{13} Jones. At room temperature, photodiodes demonstrated a dark current density of 2.2×10^{-3} A/cm^2 and a quantum efficiency of 41.5%. This work resulted in full coverage of the detection range of T2SLs from the SWIR to the very long-wavelength infrared (VLWIR) and opened the possibility of incorporating active and passive imaging in a single-chip T2SL-based focal-plane array (FPA).

Mid-Wavelength Infrared Photodetectors and Focal-Plane Arrays

Detection of electromagnetic waves in the atmospheric transparent window between 3 μm and 5 μm, usually referred to as the mid-wavelength infrared (MWIR), can be utilized for different applications such as aerial and satellite reconnaissance, target tracking using heat signals, navigation, and object identification. Similarly to SWIR T2SL photodetectors, the first challenge in realizing MWIR photodetectors is finding a proper type II superlattice design for the absorption region. Two InSb interfaces cause high mismatch when a thin InAs layer is used. Therefore, by using a highly controllable $Ga_xIn_{1-x}Sb$ ternary interface, high-quality material lattice-matched to the GaSb substrate was achieved for MWIR detection to 3.7 μm.

The main objective of MWIR photodetectors and FPAs is to operate at high temperatures (>150 K), which permits reduction of burdensome cryogenic system size, weight, and power. The obstacles to realizing high-operating-temperature (HOT) MWIR photodetectors for direct-bandgap semiconductors are the exponential increase in the minority-carrier concentration versus temperature as well as the reduction in the carrier lifetime as a result of Auger recombination at high temperatures.

To solve this problem, a tunneling barrier was designed and inserted into the junction of MWIR T2SL photodiodes,[6] resulting in a novel device structure called p–π–M–n. An M-SL with good band alignment in the conduction band with the active region was used to block the tunneling current without creating a bias dependency of the quantum efficiency. Having larger barrier potential and larger electron effective mass, the M-structure-based barrier effectively suppressed the tunneling current without affecting the photocurrent. Suppression of the tunneling allows device designers to increase the doping level of the photodiode active region to suppress the diffusion current without worrying about band-to-band tunneling around p–n junctions. A higher doping level in the active region leads to a smaller number of minority carriers, which are the source of the diffusion component of the dark current. The electrical performance of the detectors was improved by a factor of four just by increasing the doping level, while more than an order of magnitude improvement was observed with the combination of the barrier and the doping level.

Figure 1 presents the specific detectivity (D^*) spectrum of the sample with the highest doping and best performance at different temperatures with respect to the background-limited performance (BLIP) line. The device demonstrates an R_0A value of 34 kΩ cm^2 and a specific detectivity of 4×10^{12} Jones at 150 K. They were BLIP up to 195 K

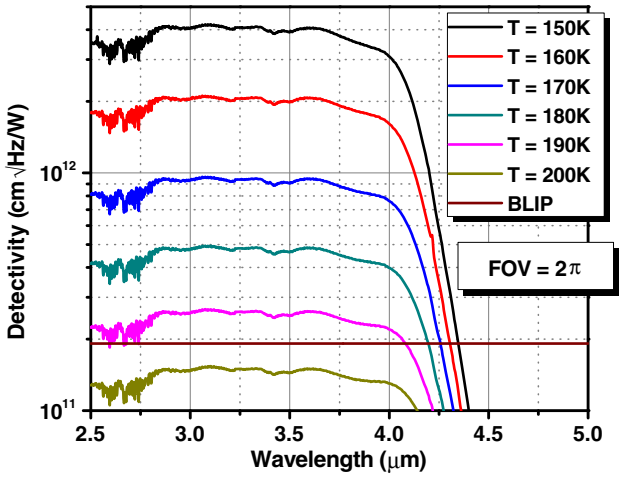

Fig. 1. Calculated detectivity spectrum as a function of temperature.

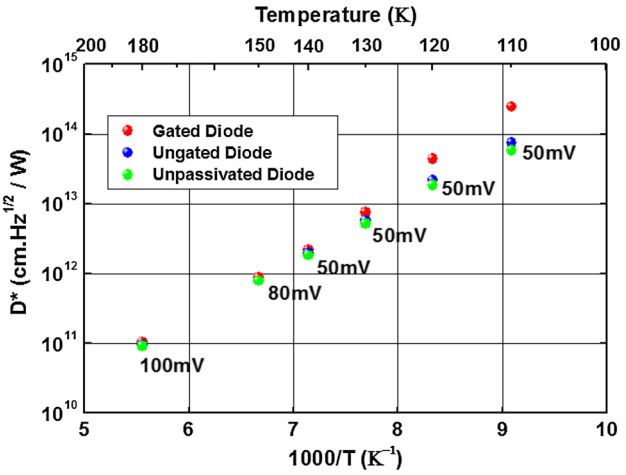

Fig. 2. Specific detectivity of an unpassivated diode, ungated diode, and gated diode at saturation gate bias at different operating temperatures.

assuming 100% quantum efficiency, 300 K background, and 2π field of view (FOV).

In addition to using different structures for optimizing the bulk performance of MWIR photodetectors to suppress the dark current density further, suppression of the surface leakage current should also be considered. Below 120 K, the bulk performance is significantly enhanced and the surface leakage caused by band-bending at the surface begins to dominate the dark current density. Leakage suppression in this range of operating temperatures is crucial for ultrasensitive applications such as astronomy. To solve the issue of band-bending at the surface of MWIR photodiodes, passivation of SiO_2 combined with the surface gating technique was used.[7] The band-bending at the photodiode side-walls can be controlled actively by applying a voltage to the gate which covers the side-walls of the photodiodes. Further details about the surface gating technique are presented in Ref. 7. At 110 K, the dark current of a gated device is reduced by more than two orders of magnitude. With a quantum efficiency of 48%, a 4.7-μm-cutoff photodiode attains a specific detectivity of 2.5×10^{14} Jones at 110 K, which is 3.6 times higher than for ungated devices (Fig. 2).

After optimization of the T2SL-based MWIR device performance, the device architecture can be used (with some modifications) to fabricate FPAs. In order to fabricate MWIR T2SL FPAs, some modifications were made to the device architecture.[6] The active region design was changed slightly to achieve a cutoff wavelength of 5 μm at 150 K. A 1.5-μm InAsSb etch-stop layer was grown prior to the photodiode growth to aid substrate removal. The MWIR FPA was hybridized to an Indigo ISC9705 readout integrated circuit (ROIC) (FLIR Systems, Goleta, CA). The FPA was mounted on a leadless ceramic chip carrier (LCCC) and loaded into a liquid-nitrogen-cooled cryostat and tested with a CamIRA infrared FPA testing system (SE-IR Corporation,

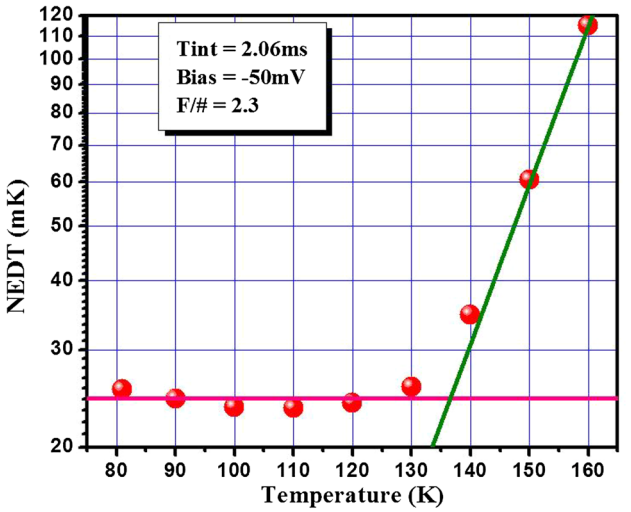

Fig. 3. FPA NETD versus operating temperature.

Santa Barbara, CA). The FPA was evaluated at operating temperatures ranging from 81 K to 150 K at a frame rate of 30 Hz.

The variation of the FPA noise-equivalent temperature difference (NETD) as a function of operating temperature is shown in Fig. 3. The NETD value stays constant up to 130 K. The NETD starts increasing at temperatures above 130 K, which causes degradation of the FPA imaging quality. However, this FPA is able to perform human body imaging up to 190 K.

Long-Wavelength Infrared Photodetectors and Focal-Plane Arrays

Going toward longer detection wavelength, the energy gap becomes smaller and the material therefore becomes more sensitive not only to the bulk properties but also to the surface trap states of

the exposed side-walls. The challenge for long-wavelength infrared (LWIR) photodetectors is to decrease the bulk dark current as well as the leakage current through the side-walls of the devices simultaneously.

A schematic diagram of a device design that combines both high optical and electrical performance is shown in Fig. 4. A strong optical response and a high quantum efficiency (>50%) were obtained thanks to a thick (6.5 μm) absorption region and high material quality. The M-structure and the double heterostructure design technique helped to reduce both the bulk dark current and surface leakage current. The device exhibited a dark current level below 5×10^{-5} A/cm^2 at -50 mV applied bias voltage at 77 K.

Using the surface gating technique,[8] surface leakage generated by SiO_2 passivation in long-wavelength infrared type II superlattice photodetectors can also be eliminated as for MWIR devices. By reducing the SiO_2 passivation layer thickness, the saturated gated bias is reduced to 4.5 V. At 77 K, the dark current density of a surface-gated device is reduced by more than two orders of magnitude, with resistance–area product of 3071 Ω cm^2 at -100 mV applied bias voltage. With quantum efficiency of 50%, the 11 μm 50% cutoff gated photodiode presented a specific detectivity of 7×10^{11} Jones, and the detectivity stayed above 2×10^{11} Jones from 0 mV to -500 mV applied bias voltage.

Based on the high-quality, high-uniformity LWIR photodiodes, a high-performance megapixel (1 k $\times$ 1 k) LWIR T2SL FPA was successfully demonstrated.[9]

Preliminary imaging results at 81 K and 68 K, with two-point uniformity correction applied, are shown in Fig. 5. The noise-equivalent temperature differences (NETDs) were measured with 20°C and 30°C backgrounds, an integration time of 0.13 ms, an *f*/2 large-format LWIR lens (StingRay Optics Co., Keene, NH), and a frame rate of 15 Hz. At a reverse bias of ~25 mV, the median NETD value was 27 mK and 19 mK at 81 K and 68 K, respectively. Figure 6 presents the NETD histograms for both operating temperatures.[10,11]

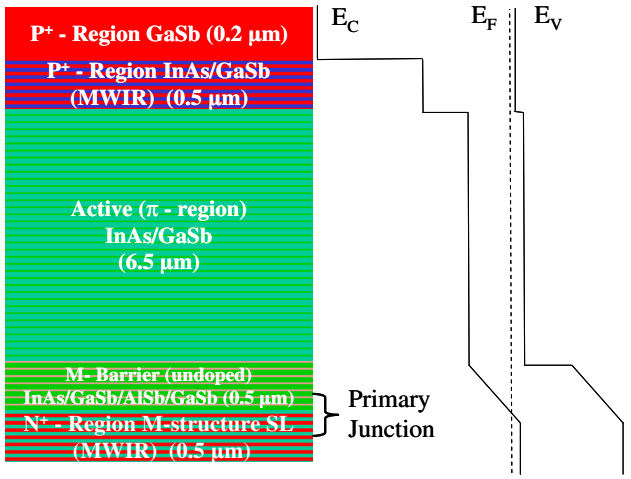

Fig. 4. Device structure and band diagram of a *p*–π–*M*–*n* superlattice photodiode. While the thicker active region increases the optical efficiency, the M-barrier and double heterostructure effectively block dark current and limit surface leakage.

HIGH-PERFORMANCE DUAL-BAND FPAS

Based on its vast experience in design, growth, and fabrication of single-band T2SL photodiodes and FPAs, the Center for Quantum Devices has demonstrated different types of dual-band T2SL-based FPAs in the LWIR,[12,13] MWIR, and SWIR regimes. The first demonstration was a high-performance 512 $\times$ 640 dual-band T2SL FPA in the LWIR regime.[13] The 100% cutoff wavelengths were 9.5 μm and 13 μm at 77 K. The imaging performance is shown in Fig. 7.

After the successful demonstration of the LWIR dual-band T2SL FPA, a high-performance 256 $\times$ 320

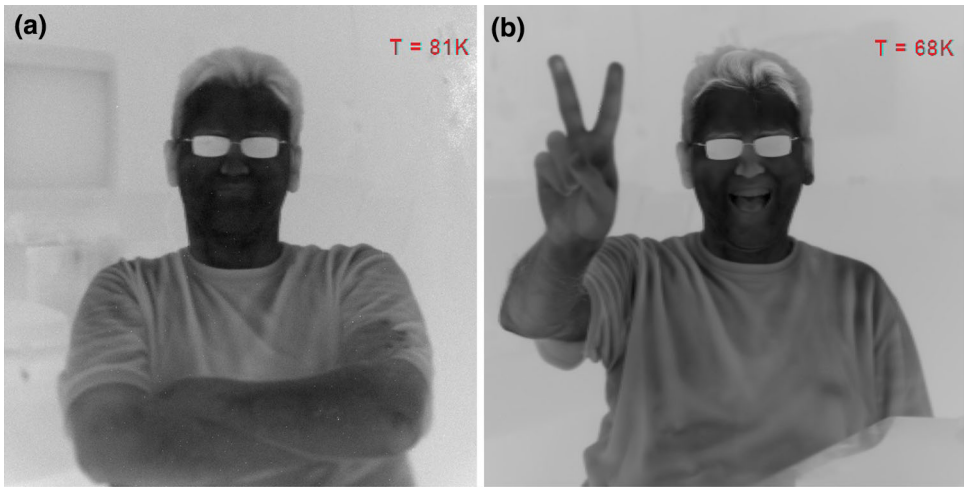

Fig. 5. Images of a student taken with the 1 k $\times$ 1 k FPA at 81 K (a) and 68 K (b).

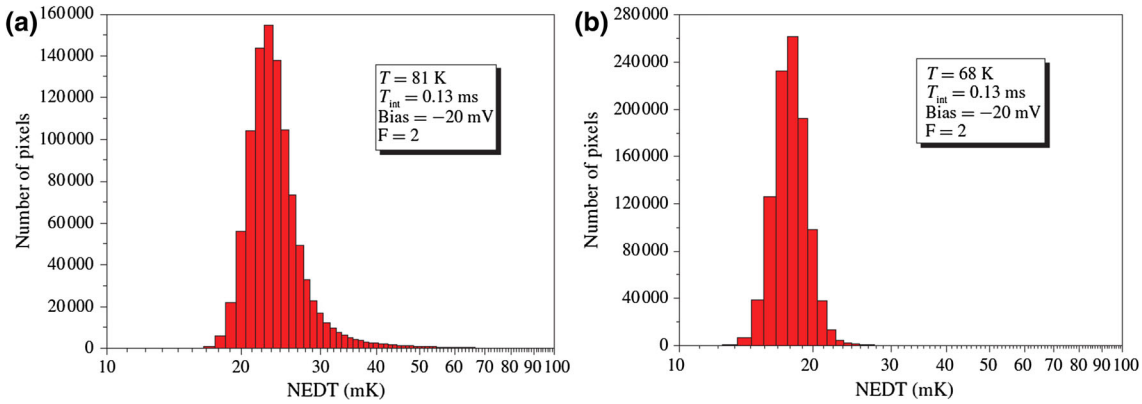

Fig. 6. 1 k × 1 k FPA NETD histograms at 81 K (a) and 68 K (b).

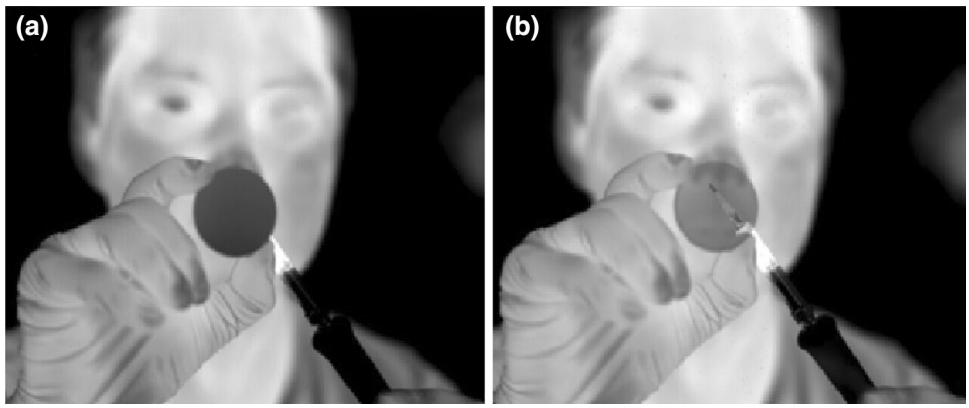

Fig. 7. Dual-band imaging using a 512 × 640 T2SL FPA with 9.5 μm (a) and 13 μm (b) 100% cutoff wavelengths at 77 K. A narrowband filter centered at 11.3 μm is placed in front of a soldering iron.

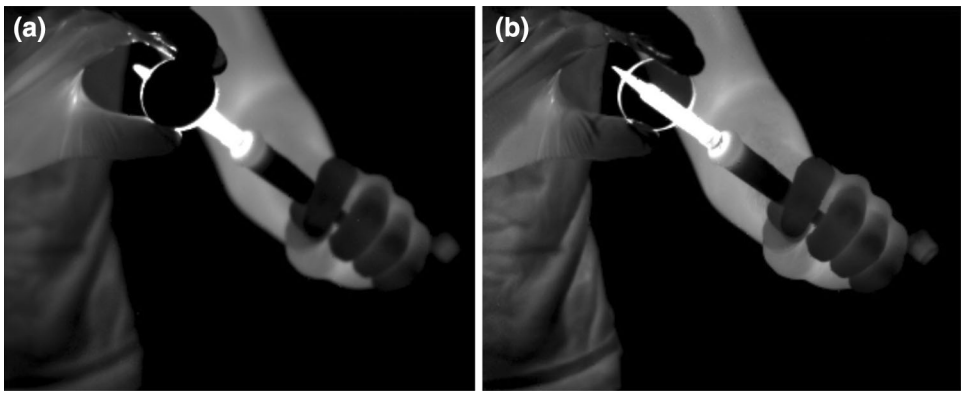

Fig. 8. Dual-band imaging using a 256 × 320 T2SL FPA with ~5 μm (a) and ~12 μm (b) 100% cutoff wavelengths at 77 K. The soldering iron covered by a narrowband filter centered at 11.3 μm has different signatures in the different infrared bands.

MWIR/LWIR T2SL FPA was demonstrated. The 100% cutoff wavelengths were ~5 μm and ~12 μm at 77 K. Details regarding this work will be elaborated in a future publication. Figure 8 shows the imaging quality of this FPA at 81 K. As shown, the soldering iron covered by the 11.3-μm narrow-band optical filter has different signatures in the MWIR and LWIR bands.[14]

These first two types of dual-band FPA performed imaging in passive mode. The new target for the

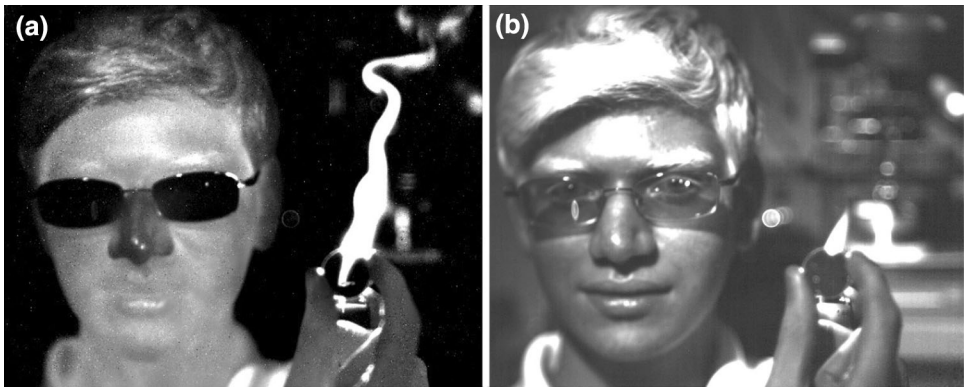

Fig. 9. Dual-band imaging using a 512 × 640 T2SL FPA with ~2.2 μm (a) and ~5 μm (b) 100% cutoff wavelengths at 150 K. The lighter's flame has different signatures in the different infrared bands. The image was taken at 120 K operating temperature.

third type of dual-band FPA was to perform both active and passive imaging in an all-in-one package. A high-performance 512 × 640 SWIR/MWIR T2SL-based FPA was demonstrated. This FPA performs both active (SWIR) and passive (MWIR) imaging in one package. The 100% cutoff wavelengths were ~2.2 μm and ~5 μm at 150 K. Details regarding this work will be elaborated in a future publication. However, the results related to a 256 × 320 SWIR/MWIR T2SL-based FPA have been published before.[15] Figure 9 shows the imaging quality of this FPA. As shown, the flame has different signatures in the SWIR and MWIR bands.

CONCLUSIONS

We present a summary of recent progress towards T2SL-based single- and dual-band photodetectors and FPAs for infrared detection in different regimes (SWIR, MWIR, and LWIR). T2SLs have been demonstrated to be an attractive low-dimensional quantum system whose theoretical limits have not yet been reached. This review of work on high-operating-temperature, megapixel, and multispectral FPAs demonstrates that this material system is making firm steps toward the era of infrared imaging and can be considered as a strong candidate to replace current state-of-the-art material systems for infrared imaging.

REFERENCES

1. G.A. Sai-Halasz, R. Tsu, and L. Esaki, *Appl. Phys. Lett.* 30, 651 (1977).
2. M. Razeghi, U.S. Patent 6864552 (2005).
3. H. Mohseni, V.I. Litvinov, and M. Razeghi, *Phys. Rev. B* 58, 15378 (1998).
4. B. M. Nguyen, M. Razeghi, V. Nathan, and Gail J, Brown (Presented at the Quantum Sensing and Nanophotonic Devices IV, San Jose, CA, USA, 2007) (unpublished).
5. A.M. Hoang, G. Chen, A. Haddadi, S.A. Pour, and M. Razeghi, *Appl. Phys. Lett.* 100, 211101 (2012).
6. S.A. Pour, E.K. Huang, G. Chen, A. Haddadi, B.-M. Nguyen, and M. Razeghi, *Appl. Phys. Lett.* 98, 143501 (2011).
7. G. Chen, B.M. Nguyen, A.M. Hoang, E.K. Huang, S.R. Darvish, and M. Razeghi, *Appl. Phys. Lett.* 99, 183503 (2011).
8. G. Chen, E.K. Huang, A.M. Hoang, S. Bogdanov, S.R. Darvish, and M. Razeghi, *Appl. Phys. Lett.* 101, 213501 (2012).
9. P. Manurkar, S. Ramezani-Darvish, B.-M. Nguyen, M. Razeghi, and J. Hubbs, *Appl. Phys. Lett.* 97, 193505 (2010).
10. A. Haddadi, S. Ramezani-Darvish, C. Guanxi, H. Anh Minh, N. Binh-Minh, and M. Razeghi, *IEEE J. Quantum Elect.* 48, 221 (2012).
11. A. Haddadi, S.R. Darvish, G. Chen, A.M. Hoang, B.-M. Nguyen, and M. Razeghi, *AIP Conf. Proc.* 1416, 56 (2011).
12. E.K. Huang, A. Haddadi, G. Chen, B.-M. Nguyen, M.-A. Hoang, R. McClintock, M. Stegall, and M. Razeghi, *Opt. Lett.* 36, 2560 (2011).
13. E.K. Huang and M. Razeghi, *SPIE Conference Proceedings* 82680Z (2012).
14. E.K. Huang, M.-A. Hoang, G. Chen, S. Ramezani-Darvish, A. Haddadi, and M. Razeghi, *Opt. Lett.* 37, 4744 (2012).
15. E.K. Huang, A. Haddadi, G. Chen, A.-M. Hoang, and M. Razeghi, *Opt. Lett.* 38, 22 (2013).